H. Ax, P. Kutne, W. Meier, K. König, U. Maas, A. Class, M. Aigner, Low Pressure Premixed CH4/Air Flames with Forced Periodic Mixture Fraction Oscillations: Experimental Approach, Applied Physics B: Lasers and Optics 94 (2009) 705–714.

The original publication is available at www.elsevier.com

http://dx.doi.org/10.1007/s00340-009-3372-8

Low Pressure Premixed CH$_4$/Air Flames with Forced Periodic Mixture Fraction Oscillations: Experimental Approach

H. Ax[1], P. Kutne[1], W. Meier[1], K. König[2], U. Maas[2], A. Class[3], M. Aigner[1]

[1] Institute of Combustion Technology, German Aerospace Center (DLR), 70569 Stuttgart, Germany, (Fax +49 711 6862 578)
[2] Institut für Technische Thermodynamik, Universität Karlsruhe, Kaiserstrasse 12, 76128 Karlsruhe, Germany
[3] Institute for Nuclear and Energy Technologies, Forschungszentrum Karlsruhe GmbH, 76021 Karlsruhe, Germany

Abstract An experimental setup for the generation and investigation of periodic equivalence ratio oscillations in laminar premixed flames is presented. A special low pressure burner was developed which generates stable flames in a wide pressure range down to 20 mbar and provides the possibility of rapid mixture fraction variations. The technical realization of the mixture fraction variations and the characteristics of the burner are described. 1D laser Raman scattering was applied to determine the temperature and concentration profiles of the major species through the flame front in correlation to the phase-angle of the periodic oscillation. OH* chemiluminescence was detected to qualitatively analyze the response of the flame to mixture fraction variations by changing shape and position. Exemplary results from a flame at p = 69 mbar, forced at a frequency of 10 Hz, are shown and discussed. The experiments are part of a cooperative research project including the development of kinetic models and numerical simulation tools with the aim of a better understanding and prediction of periodic combustion instabilities in gas turbines. The focus of the current paper lies on the presentation of the experimental realization and the measuring techniques.
PACS: 33.20.Fb; 47.70.Pq; 47.80.Fg

1 Introduction

The design of modern gas turbines follows the concept of lean premixed combustion in order to reduce NO$_x$ emissions [1,2]. However, such systems are prone to thermoacoustic instabilities driven by the combustion process and sustained by a resonant feedback mechanism coupling pressure and heat release [3–7]. The oscillating pressure affects the fuel and air supply rates, which

Send offprint requests to: Holger Ax
Correspondence to: holger.ax@dlr.de

can lead to equivalence ratio oscillations due to different impedances of the supply lines. This feedback loop is known as oscillating fuel supply combined with a convective time delay [8–13]. The periodic equivalence ratio oscillations have, of course, an impact on the chemical and physical processes within the reaction zone and the extent depends on the amplitude and frequency of the oscillation and also on the combustion pressure, temperature and some other parameters.

It is expected that at low oscillation frequencies the flame can immediately follow the changes in gas composition. At very high frequencies, the flame will presumably not respond to the changes but rather "see" a temporally averaged composition. In the range of intermediate frequencies, different effects of the coupling between transport and chemistry may occur. These different flame responses to mixture fraction oscillations have already been observed in numerical studies [14–18]. In simulations of counterflow or stagnation point premixed flames subjected to composition oscillations, a quasi-steady flame response at sufficiently slow frequencies was found and also a "cutoff frequency", beyond which the reaction zone no longer responds to the imposed oscillations. In the intermediate to higher frequency range the flame could be sustained even if the equivalence ratio fell below the steady flammability limit during a cycle.

In order to account for the effects of equivalence ratio oscillations on the kinetics and dynamics of the flame in numerical simulations of technical flames, the University of Karlsruhe, the Research Center Karlsruhe and the German Aerospace Center DLR started a research project within the Collaborative Research Center 606. A combustion model based on the levelset method is developed at the Research Center Karlsruhe [19–23]. This model includes detailed chemical kinetics, which is modeled and investigated at the University of Karlsruhe [17, 18]. An analysis of the perturbation of premixed flames using this model also revealed the quasi-steady state behavior at low frequencies and a response of the flame

only to an averaged value of the mixture composition for high frequencies, which results from an equilibration of the mixture composition waves before they reach the flame. Simulations at low pressure during this work have been the basis for the design of the experiment to ensure that measurements could be performed in the frequency range of interest from the quasi-steady response to higher frequencies. The experiments are performed at DLR in order to determine boundary conditions for the numerical simulations and to validate the developed models. In the present paper, the focus is on the experimental approach.

The burner, that was designed for the experiment, stabilizes a premixed CH_4/air Bunsen flame with a diameter of 40 mm and enables pulsed injection of additional CH_4 through an array of small tubes implemented in the burner. In order to simplify the experiment, the measurements were performed in a low pressure flame at 69 mbar. The reduced pressure yields several advantages. (1) The reaction zone widens to a thickness of several millimeters and can thus be spatially resolved by laser measuring techniques. (2) The chemical reaction rate is reduced by approximately two orders of magnitude in comparison to gas turbine flames at high pressure. Therefore, the time scale of the equivalence ratio oscillation can also be reduced from the order of 1 kHz to the order of 10 Hz. At such a low frequency the periodic variation of the equivalence ratio can be achieved under well-defined laminar conditions. (3) At reduced pressure, the relatively fast molecular diffusion can be exploited to achieve a homogenization of the fuel/air mixtures in horizontal direction.

In order to investigate the response of the reaction zone to the periodic changes of the equivalence ratio, 1D laser Raman scattering was applied. This technique enables the simultaneous determination of the major species concentrations (CH_4, O_2, N_2, CO_2, H_2O, CO, H_2) and the temperature along a line [24–26]. In the setup employed here, the laser beam was irradiated along the axis of the burner and the section intersecting the flame front was imaged onto the detector. By triggering the laser and detector in correlation to the pulsed CH_4 injection, phase-resolved measurements of the variations of the species and temperature profiles could be performed. As the configuration enabled a very stable and reproducible operation, Raman signals could be averaged over several hundred laser shots.

The main goals of the paper are the presentation of a combustor for lean, premixed low pressure flames, which allows for inducing oscillations of the equivalence ratio Φ, and a characterization of the flame response to variations of Φ. The paper describes the experimental arrangement for 1D laser Raman scattering and OH* chemiluminescence measurements in a low pressure flame and presents exemplary results from phase-resolved measurements at an oscillation frequency of the equivalence ratio of 10 Hz. Experimentally determined concentration profiles through

the flame front are shown and compared to the results of the numerical simulation of the detailed chemistry. The emphasis in this paper lies on the demonstration of the successful realization of the experimental concept and the suitability of the experimental methods. The focus is not on the presentation of oscillation-induced combustion phenomena or the validation of physical or chemical models. This will be the topic of upcoming papers.

In further steps, an experimental data base for the validation of numerical flame simulations will be established, including the detailed characterization of flame response to equivalence ratio oscillations of different frequencies and amplitudes. The chemical kinetic and hydrodynamical flame models developed within the cooperative research project are published in forthcoming papers, as well as the detailed comparisons of the experimental and the numerical results.

2 Experimental Setup

2.1 Low pressure burner and flames

The burner was designed to fulfill two objectives. One was the generation of a stable laminar premixed flame under low pressure conditions, the second was the feasibility of inducing variations of the equivalence ratio Φ to the laminar flame. A schematic drawing of the burner is shown in Fig. 1. A gas flow of premixed CH_4/air (light blue) for the laminar flame exits a central outlet with a diameter of 40 mm. The nozzle for this main flow is convergent over the last 34 mm to the exit in order to smooth out the flow velocity profile to an even distribution for a straight flame cone. This Bunsen-type burner is surrounded by an annular water cooled bronze matrix burner (i. d. = 42 mm, o. d. = 70 mm), operated with a premixed CH_4/O_2 flame (dark blue). By this flat flame, the inner flame is stabilized on the burner mouth in a wide range of pressure and equivalence ratio. In tests, flames could be stabilized at pressures down to 20 mbar. The typical settings for the undisturbed stationary flame were an air mass flow of 5.17 g/min and a CH_4 mass flow of 0.26 g/min ($\Phi = 0.86$) at an absolute pressure in the combustion chamber of 69 mbar. The picture in Fig. 1 on top of the burner sketch shows the appearance of such a flame, which exhibits relatively straight cone shoulders and a rounded tip. From the given settings and geometry the mean flow velocity was derived as 964 mm/s at an inlet temperature of 310 K. If the flame shape would be considered as a perfect cone, the laminar flame speed would be determined to 680 mm/s as the normal component of the velocity of the unburned mixture, which approaches the flame front at an angle of 45°. This value for the flame speed is higher than at atmospheric pressure as expected due to the increased diffusional transport at low pressure.

The equivalence ratio of the inner flame can be varied by an additional pulsed CH_4 flow, fed through 48

tubes, which are placed in the plenum of the inner flame (marked red in Fig. 1). The tubes have an inner diameter of 1 mm and are shower head like arranged with a distance of 4.5 mm in between. The pulsed CH_4 flow was realized by a magnetic 3/2-way valve placed in the tubes' common inward flow. The pull-in- and drop-out-times of the valve are below 1 ms. The influence of the valve reaction time on the slope of the CH_4 concentration gradients is therefore negligible compared to the effects of molecular diffusion inside the tubes and from their outlet to the flame front. The pulse duration was set to half the period time (50 ms at 10 Hz), which, by the effect of diffusive transport, resulted in an approximately sinusoidal pulse form when reaching the flame front. The additional pulsed CH_4 mass flow was set to 0.014 g/min for the flames which are described in this paper, which resulted in an overall equivalence ratio of $\Phi = 0.91$ for the interval of a pulse.

The distance from the open end of the tubes to the burner outlet can be adjusted for different flow and pressure conditions to ensure a horizontal homogeneous distribution of the additional CH_4 in the main flow within that distance by diffusive and convective transport. In the direction of flow, a spatial variation of Φ is achieved, depending on diffusion velocities and the settings for pulsation and mass flow.

For typical flame settings as described above, the change in the upstream flow velocity due to the additional pulsed methane is 0.4 % compared to the constant premixed flow and therefore neglegible. Assuming a constant velocity across the burner, the flow covers a distance of 96.4 mm in the time of one cycle at a pulsation frequency of 10 Hz, which is referred to as the "wavelength". From the open end of the pulsation tubes, located 9 mm below the burner exit, to the flame tip at a height above the burner (HAB) of 20 mm it takes the gas mixture $t = 30$ ms. During this time, the pulsed methane out of the tubes covers the distance x_D of 4.6 mm by diffusional transport, based on the simple approximation $x_D = sqrt(2\,D\,t)$, where D is the diffusion coefficient, which was determined to $D = 3.5\,cm^2/s$ for CH_4 in air at a pressure of 69 mbar. During the time it takes the flow from the tubes' end to the burner mouth, the distance by diffusional transport is 2.5 mm, which is sufficient to smooth out the gradients in horizontal direction between the tubes. The pulse distribution of the CH_4 pulse after exiting the tubes was investigated using Raman scattering of a laser sheet and is described in more detail in the following. Other techniques were not used as they would have involved excessive experimental complexity. Laser induced fluorescence of a tracer was not used because an appropriate tracer with the same diffusion coefficient as CH_4 in air in order to investigate the effect of the diffusional transport correctly was not found. Rayleigh scattering was difficult to apply in the combustion chamber as there was a lot of background illumination from reflections on the entrance and exit windows and on the

inner walls of the small laser duct tube in the middle of the burner. For the same reason, Rayleigh scattering was also not applied to measure the temperatures across the flame front.

All gas flows were controlled by mass flow controllers (Brooks) with specific operating ranges; CH_4 and O_2 were fed from pressurized bottles, dry air was supplied by an in-house pressure line.

A thermocouple (type K) measured the temperature of the premixed CH_4/air flow at the position of the tubes outlet, 9 mm below the burner mouth. This temperature is used as a boundary condition for the numerical simulations and did not exceed 310 K for a burner operation time of several hours. A screen with a wire diameter of 0.4 mm and a free area coefficient of 0.64 is placed at the burner outlet and prevents flash back.

A tube with an inner diameter of 4 mm in the center of the burner serves as a laser duct allowing for 1D laser Raman scattering measurements in the direction of flow for investigations of the flame structure. The open end of the tube inside the burner is 20 mm below the outlets of the pulsation tubes in order not to disturb the flow field. The other end outside the burner is sealed by a plane plate, which is glued onto a flange in the Brewster angle in order to minimize reflections of the entering laser beam.

2.2 Low pressure chamber

The burner is pressure-tight inserted in the bottom of a cylindrical combustion chamber (i. d. = 318 mm), mounted by an ISO-K DN 100 flange. The burner itself is adjustable in height relatively to the mount flange to allow for laser spectroscopic measurements in the flame at different heights above the burner while keeping the same optimum solid angle for detection. The combustion chamber with a volume of $0.025\,m^3$ also serves as a low pressure vessel. A pump (Leybold-Heraeus D40BCS) evacuates the chamber through the exhaust line which is flange mounted onto the lid of the chamber. The throughput of the pump is constant, sufficient to reach pressures inside the chamber of less than 1 mbar. The pressure is PID-software controlled by reading out the actual pressure, measured by two flange mounted sensors (Transamerica Instruments BHL-4201-00-03 and MKS 627BX12TDC1B), and automatically adjusting an orifice valve, which is installed in the suction line between pump and exhaust flange. The desired target pressure is achieved with an accuracy of 0.5 mbar. The oscillating CH_4 mass flow in this experiment was too small to effect the pressure regulation. Different pressure ranges can be achieved by setting a constant air mass flow, which enters the chamber through an annular channel on the bottom of the chamber around the burner. A typical mass flow of this air co-flow was 15 g/min which corresponds to a controllable pressure range inside the combustion chamber from

30 mbar to 100 mbar. This co-flow also serves for cooling the chamber walls and has no effect on the flame. ISO-K DN 100 flanges around the chamber allow for mounting windows pressure-tight to the vessel for optical access.

2.3 1D laser Raman system

The Raman scattering process is very weak with cross sections in the order of 10^{-31} cm^2/sr and the intensity of scattered light is linearly proportional to the species number density [24]. Therefore, the biggest challenge of applying Raman scattering measurements on combustion under low pressure conditions is to obtain a sufficient signal to noise (S/N) ratio. This can be achieved with high energy density in the incident laser beam. In this experiment, we used six frequency-doubled pulses ($\lambda = 532$ nm) of three double-pulse Nd:YAG laser systems (Spectra-Physics PIV 400), which were spatially overlaid, temporally stretched and directed vertically through the laser duct in the center of the burner. The laser system and the detection optics for 1D Raman scattering measurements had already successfully been used on a gas turbine combustor at elevated pressure [26]. For the experiment described in this work, the system was slightly modified. A new pulse stretcher was used to reduce the intensity peaks in order to prevent optical breakdown at the focus and to protect the optical components from damage. A schematic drawing of the pulse stretcher is displayed in Fig. 2. Two beam splitters and six mirrors route portions of each pulse ($\sim$8 ns) along three different pathways of different distances and recombine them to one pulse train. By this and appropriately triggering the Q-switches of the lasers, a pulse train with a duration of $\sim$350 ns and an effective energy of around 900 mJ could be used for the measurements. A small amount of the beam was reflected by a wedge plate right after the pulse stretcher and focused onto a CCD position measuring system (DUM-SpotOn-CCD) to monitor the profile and spatial overlapping of the pulse train. A photo diode tracked the laser intensity in time. A spherical lens with a focal length of 2 m focused the laser beam to a waist thickness of 0.4 mm in the area of investigation right above the burner outlet. The transmitted fraction of the beam through the last mirror in front of the entrance into the laser duct was directed to a power meter to monitor the laser energy. A second power meter was placed behind the window through which the beam exited the chamber upwards. The comparison of both measured laser energies allowed for determining whether there were energy losses inside the chamber, such as a stained entrance or exit window, or by contact of the beam with the walls of the narrow duct.

The components on the detection side were the same as used in [26] with some different settings. The Raman signal was detected normal to the polarization plane of the incident beam. The vertically directed measuring volume of 7 mm length and 0.4 mm diameter was imaged by an achromatic lens system (aperture 150 mm) onto the entrance slit of the spectrograph (Acton Research, SpectraPro 300i, f = 300 mm, 490 grooves/mm, $f_\# = 4$, dispersion $\sim$6 nm/mm, coverage 163 nm) with an image magnification of 2. The elastically scattered light was separated out by a holographic notch filter in front of the slit. The spectrally resolved Raman bands of the major species (N$_2$, O$_2$, CH$_4$, CO$_2$, H$_2$O, CO and H$_2$) were recorded by an intensified CCD-camera (Princeton Instruments PI-MAX, Gen III intensifier, 1340x1300 pixels), which was flange mounted to the spectrograph. A range of 1340x700 pixels was binned on chip (5x25) to 268 points on the spectral axis and 28 points on the spatial axis, yielding a spatial resolution of 28 scattering volumes of 0.25 mm length and 0.4 mm diameter. The gate width of the camera was set to 1 μs. The laser and camera triggers could be set to arbitrary phase angles in a period of the CH$_4$ pulsation at any frequency by a frequency divider and a time delay relative to the CH$_4$ valve trigger.

2.4 Raman signal reduction

To derive the number density n of a molecular species i in a measurement volume, the rotation-vibrational Raman signal intensities were integrated over a specific spectral range and evaluated by

$$n_i = \frac{P_i}{P_L \cdot (d\sigma_i/d\Omega) \cdot \Omega \cdot L \cdot \epsilon \cdot q}. \qquad (1)$$

Herein is P_i the power of the scattered Raman signal, P_L the incident laser power, $d\sigma_i/d\Omega$ the differential Raman cross section, Ω the detected solid angle, L the length of the measurement volume, ϵ the transmission efficiency of the detection optics and q the quantum efficiency of the detector [27]. For a quantitative evaluation of gas compositions at different temperatures and mixture fractions, a calibration is needed. Therefore, the Raman signals of pure N$_2$, CO$_2$, CO, H$_2$, CH$_4$ and air were measured at different known temperatures in the range from 293 to 1000 K at atmospheric pressure. The gases were heated by an electrical gas heater. The temperatures were measured by a thermocouple. In addition, calibration measurements were made in the post-flame region of both CH$_4$/air and H$_2$/air flat flames. The calibration burner was made of a sintered porous bronze matrix with a diameter of 42 mm. The matrix was cooled by an inner water conduit and surrounded by an annular matrix with an outer diameter of 56 mm, providing the possibility for a stabilizing co-flow. The temperatures of the flames were determined by in-house CARS measurements, the species concentrations were deduced from equilibrium calculations with the software Gaseq v0.79 [28]. Both the gas heater and the calibration burner were flange

mounted onto the low pressure chamber to allow for calibration measurements at the actual location of the low pressure flame. By this calibration procedure, temperature dependent effects of the vibrational Raman bands on the detected signal like broadening and shifting as well as optical effects of the detection optics were taken into account by the determination of calibration coefficients $G_i(T)$. The temperature dependent bandwidth factor $f_i(T)$ was reduced to the molecular Boltzmann population distribution

$$f_i(T) = \frac{1}{1 - \exp(\frac{-hc\nu_i}{kT})}, \qquad (2)$$

where ν_i is the wavenumber of the vibrational state v_i, and h, k and c are the constants of Planck and Boltzmann and the speed of light in vacuum, respectively [24, 27]. The detected signal intensities P_i were corrected from spectral overlap of different species, the so called crosstalk effect, yielding $P_{c,i}$. Eq. 1 could then be rewritten to

$$n_i = \frac{P_{c,i}}{P_L \cdot k_i \cdot f_i(T) \cdot G_i(T)} \qquad (3)$$

with a constant k_i, combining all constants in Eq. 1. The total particle density n in a probed volume was approximated by the sum of the molecular density numbers n_i of the detected major species. The pressure p was known by sensor probing. Thus, the temperature could be deduced by the ideal gas law $T = p/nk$. All the calibration measurements and the measurements on the low pressure flame were averaged over 300 single shots and corrected for background luminosity and minor optical effects by normalizing the signal according to a daily reference signal of dry air at known pressure and temperature. The known linear and nonlinear effects of incident laser intensity, pressure and intensifier gain on the signal were taken into account by normalizing the signal to reference values.

2.5 Uncertainty of 1D-Raman measurements

The basis of the evaluation procedure is the calibration data set. For each species, it contains polynomials describing the dependency of the detected signal in a species specific spectral range on the temperature as well as temperature dependent polynomials for the cross talk of one species into another. The calibration coefficients G_i have the most influence on the accuracy of the measurements since there are uncertainties in the temperature and species concentrations. This is especially the case for the high temperature range, where the Raman signals are calibrated by flames in which some species concentrations are very small and also sensitive to the mixture composition. The deduced maximum uncertainties of G_i from representative calibration flames are given in the following. The determination of

G_i is based on the integrated signal in the species specific spectral range, the temperature, the species concentration, the laser intensity, the pressure and the bandwidth factor. The temperature of the calibration flames were measured by coherent anti-Stokes Raman scattering (CARS) with an uncertainty of less than 3 %. The pressure inside the combustion chamber was determined with an uncertainty of 1 %. The laser intensity for the 1D-Raman measurements, averaged over 300 single shots, was detected with a relative standard deviation of 1 %. However, the Raman signal was seen to vary by an additional 2 % over the course of a day due to effects of beam drift or thermal imbalance of the laser system. Measurements on atmospheric air were taken each day before and after the flame measurements to account for these effects. Uncertainties in the equilibrium gas composition of a calibration flame arise from fluctuations and calibration uncertainties of the mass flow controllers (2 %) and from the uncertainty of the measured temperature using CARS. Taking all this into account, the calibration coefficients G_i, deduced from a lean flame ($T_{ad} = 1996$ K, $\Phi = 0.8$, atmospheric pressure), were determined with a relative uncertainty of ~4 % for N_2, H_2O and CO_2 and 13 % for O_2. The uncertainties of G_i for CO and H_2 were deduced from a rich flame ($T_{ad} = 2137$ K, $\Phi = 1.2$, atmospheric pressure) and were determined with a relative uncertainty of 25.6 % for CO and 22.4 % for H_2. The uncertainties for O_2, CO and H_2 are primarily due to the sensitivity on the gas composition and the relatively low absolute mole fractions in the burned gas of the regarded flames of around 4 % for O_2 and CO and 2 % for H_2. The detected Raman signals of O_2 and CO in the burned gas were also subject to crosstalk effects from CO_2 and N_2, respectively. The relative uncertainties of the calibration coefficients that were deduced from measurements in cold and electrically heated gases were less than 4 % for all gases.

With the known uncertainties of G_i the maximum uncertainties of the particle densities n_i in a low pressure flame using Eq. 3 could be calculated by propagation of error. The uncertainties of the mean values of the mole fractions are 5.7 % for N_2, 13.9 % for O_2, 6.8 % for CO_2, 5.8 % for H_2O, 23.6 % for H_2, 50.6 % for CO (all in the burned gas) and 5.6 % for CH_4 (fresh gas). The reasons for the relatively high uncertainties of O_2, H_2 and CO are the uncertainties of the according calibration coefficients, the crosstalk effects by other species and the low absolute mole fractions. The temperature is determined with an uncertainty of 4 % in the preheat zone.

The effect of the reduced S/N ratio at low pressure is relatively small due to the averaging over 300 single shots. Compared to measurements at atmospheric pressure, the uncertainties of the mean values due to shot noise of the detected photons at 69 mbar are increased by, for example, 0.2 percentage points for the N_2 mole fraction, 1.3 percentage points for the CO_2 mole fraction and 0.2 percentage points for the temperature.

2.6 OH* Chemiluminescence

Chemiluminescence arises from electronically excited radicals, such as OH*, CH*, C_2* or CO_2*, which are formed during chemical reactions in flame regions of high heat release. The excitation of a molecule is released by spontaneous emission of a photon. Chemiluminescence has widely been employed for the determination of heat release rate and the flame front position or motion [29–31]. Smith et al. [32] investigated absolute OH* concentrations in low pressure CH_4/air flames. In the experiment described here, chemiluminescence of the OH* radical was detected to qualitatively determine the shape and position of the flame and the phase correlated movement during mixture fraction oscillations. An intensified camera (PCO DiCam2, 767x288 pixel, gate width $250\,\mu s$) detected the emitted light right-angled to the Raman detection line through a quartz window. The same camera trigger was used as for the Raman signal detection. The collection optic was a camera objective (Nikon UV-NIKKOR, 105 mm) equipped with a bandpass filter in front of it, which transmits light in the range from 290 nm to 335 nm. As for the Raman scattering measurements, the chemiluminescence images were averaged over 300 single shots and corrected for background luminosity and chip sensitivity. Due to the rotational symmetry of the flame, the 2D images of the integrated signal could be deconvolved by a three-point Abel inversion to derive a section of the symmetry plane through the flame tip [33].

2.7 Boundary conditions / pulsed CH_4-flow

For the numerical simulation, the oscillation of the CH_4 concentration is approximated by a sinusoidal change of the CH_4 mass flow at the burner outlet, assuming a horizontal homogeneous distribution of the CH_4 pulse. This was also considered for the burner design and the arrangement of the pulse tubes and is accomplished by utilizing the effects of diffusional transport normal to the flow direction. The validity of the assumption was investigated and confirmed by measuring the Raman scattered light from CH_4 in horizontal direction. For this study, the same three double pulse laser systems as for the 1D Raman measurements were used to form a laser sheet of ~3 mm height as a trade-off between the extent of the imaged area and a high laser energy density for sufficient Raman signal ($\lambda = 532$ nm, pulse energy ~900 mJ). The outlets of the tubes, through which the pulsed CH_4 is induced into the premixed flow, were positioned ~3 mm above the burner in order to investigate the spreading of the CH_4 right after streaming out of the tubes. The laser sheet was directed horizontally over the tubes allowing for measurements at heights above the tubes from 1.9 mm on. Figure 3 shows schematically the guidance of the laser sheet and the position of the imaged area above the tubes. The laser beam was narrowed by a cylindrical plano-convex lens ($f = 400$ mm) and parallelized by a cylindrical plano-concave lens ($f = -110$ mm). In the line of sight, the sheet was focused by a cylindrical plano-convex lens with a focal length of 750 mm to a minimum thickness of 0.5 mm. The Raman scattered light was filtered by a bandpass filter with a transmission range from 620 to 640 nm, placed in front of the camera, to separate the signal of CH_4 from the signal of other species and Rayleigh scattering. With an on-chip binning of 10x10 pixels and a magnification of 1.75, the spatial resolution was 0.11×0.11 mm^2 per superpixel. Calibration measurements on gas mixtures of different known mole fractions (without pulsation) were made to determine the correlation between signal intensity per pixel and molecule density. A quantitative evaluation of measurements with unknown mixture fractions was possible due to known pressure and temperature at the tubes' outlet. For the period of the pulse characterization by 2D-Raman scattering, daily reference measurements were acquired for normalization of the signal to the corresponding level of the calibration measurements and to correct the images for the effects of unequal laser intensity distribution along the sheet height. Only pixels inside the range of FWHM-intensity were evaluated. This resulted in total to an analyzed area of 14.74 mm in horizontal and 2.2 mm in vertical direction, covering the outlet of three tubes. However, the reduced energy density compared to 1D Raman scattering led to a small S/N ratio. The gradients of the intensity distribution in the laser sheet were quite high and not constant over one day due to the usage of six single shot lasers and therefore strong effects of beam drift. This resulted in a relative uncertainty about the absolute CH_4 mole fractions of around 10 % in the case of measurements at atmospheric pressure and around 20 % at 69 mbar.

3 Results and Discussion

The spreading of the pulsed injected CH_4 was analyzed by the evaluation of the CH_4 concentration in the horizontal direction at different heights above the tubes with 2D laser Raman scattering. An example of the results is shown in Fig. 4. In the diagram, the CH_4 mole fraction at two different heights above the tubes is plotted against the horizontal position. The measurements were conducted at a pressure of 69 mbar. The mass flow through the inner flame was 5.43 g/min as for the actual flame investigation; the pulsed CH_4 mass flow in both measurements was 0.072 g/min, i. e. five times higher than for the actual flame investigation. This was necessary because the actual pulsation of 5.2 % of the constant CH_4 mass flow was too small to be sufficiently revealed by 2D-Raman scattering. At a height of 2.4 mm above the tubes, an unequal CH_4 distribution is clearly visible, with higher concentrations above the tubes. At 3.5 mm,

the CH_4 has already spread more in horizontal direction by diffusional and convective transport, so there are far smaller gradients in the CH_4 distribution. The lower average value of the mixture fraction at 3.5 mm is due to the mentioned difficulties with the correction of the intensity distribution in the laser sheet. Despite of the high measurement uncertainty of the CH_4 concentration due to the low S/N ratio, the planar Raman scattering allows qualitative conclusions even at low pressure. The burner design and the assumption of an equal horizontal pulse distribution as a boundary condition for numerical investigation could therefore be approved within the distance from the tubes' end to the burner outlet (9 mm).

The OH* chemiluminescence measurements revealed the shape and position of the low pressure flame. Figure 5 shows averaged and deconvolved images of the OH* distribution in the flame at two phase angles of the pulsed mixture fraction oscillation. The flame settings were a total premixed mass flow of 5.43 g/min ($\Phi = 0.86$) and a pulsed CH_4 mass flow of 0.014 g/min at a frequency of 10 Hz. The results were averaged over 300 phase locked single shots. For better comparison, the images of the two different phase angles are cut along the symmetry axis and plotted from the flame tip to the left and right, respectively. The phase angles are related to the periodical displacement of the flame due to the changing flame velocity with varying mixture composition. 0° (left image) refers to the phase angle with the maximum distance of the flame front from the burner mouth during one period. The image on the right (180°) shows the OH* distribution at the minimum distance, which is half a period later. One can see the shape of the flame from the flame tip to the shoulder where it is anchored by the flat stabilization flame. The flame tip is closer to the burner than at 0° due to an increased flame speed with increased equivalence ratio Φ. The total displacement of the flame tip between the two positions is around 1.5 mm. The OH* distribution showed hardly any variances in the single shots at one phase angle, which confirms the stability of the flame and the reproducibility of its response to periodical variations of the mixture fraction. The thickness of the OH* distribution of around 2 mm arises from the widening of the flame front at low pressure. The exposure time of 250 μs for the OH* detection results in an uncertainty of the flame position of 0.01 mm, assuming that the flame covers a distance of 1.5 mm in 50 ms.

The structure of the flame between the unburned and burned gas was investigated by 1D Raman scattering. An example of the 1D Raman results is shown in Fig. 6 for the same flame and pulse conditions as for the OH* chemiluminescence results. In the diagram, the mole fractions of the major species CO_2, O_2, CH_4, H_2O, CO and H_2 across the flame front are plotted against the height above the burner (HAB) at an oscillation phase angle of 0°, i.e. at maximum distance of the flame tip from the burner mouth. In order to demonstrate the

agreement between experiment and simulation which is typically achieved, the experimentally determined concentration profiles (symbols) are compared to the values obtained from a one-dimensional simulation of the detailed chemistry (lines). From left to right, one can see the consumption of the reactants CH_4 and O_2 and the formation of the products CO_2 and H_2O, where the kinetic model is in good agreement with the experiment for all species. Only in the region of the burned gas there is a discrepancy between the measured and numerically calculated concentrations of CO and CO_2. The numerical simulations were carried out for laminar, premixed and stretched counterflow flames using the simulation code INSFLA, a one-dimensional code for the simulation of instationary flames [34]. Time-dependent boundary conditions for the CH_4 mass fraction were used to simulate the periodic CH_4 concentration oscillations. All parameters of the simulation such as system dimension, pressure etc. as well as the degrees of freedom of the time-dependent boundary condition (frequency, mean equivalence ratio and amplitude) were adjusted according to the experimental setup. Detailed chemistry (34 species) [35] and a detailed transport model ($Le \neq 1$ and non-equal diffusivities) were used; effects of flame stretch were taken into account. More detailed descriptions can be found in [17] and [18]. The result of the calculations is a time-dependent vector of thermokinetic state variables, e.g. enthalpy, pressure and mass fractions of the species, at each spatial location of the calculation domain, which can be compared to the results of the experimental measurements.

The flame response to mixture fraction oscillations becomes evident by comparing the concentration profiles at different phase angles, acquired by 1D Raman measurements. In Fig. 7 the mole fractions of CH_4 and H_2O across the flame front are plotted against the HAB for the phase angles of 0° and 180°, i.e. at maximum and minimum distance of the flame front from the burner, at a pulse frequency of 10 Hz. The indicated lines are fit curves using a Boltzmann growth function. At 0°, the curvature of the CH_4 profile begins to change from almost horizontal at HAB = 18.5 mm and reaches the maximum slope at around 21.75 mm. The concentration of water at the same phase angle starts with a value of 0 % and reaches the maximum slope at 22.25 mm. With increasing CH_4 concentration in the unburned gas due to the methane pulse, the flame speed increases and the flame front moves towards the burner. At 180°, the position of the flame is closest to the burner, with the highest concentration gradients at a HAB of around 20.25 mm for CH_4 and 20.75 mm for H_2O. The displacement of the flame front between 0° and 180° of around 1.5 mm is well detectable and rather distinct considering the relatively small variation of the CH_4 concentration. The detected displacement is also in agreement with the observation from the OH* chemiluminescence. Due to the displacement of the flame, the region of the profiles with

a horizontal slope in the preheat zone are out of the detection range. After the pulse, the CH_4 concentration decreases again and the flame front moves away from the burner until it changes the propagation direction again at 0° after a complete cycle. The fit curves help to determine the CH_4 concentration in the fresh gas which is not detected in the plotted range of the HAB. During one cycle, the CH_4 mole fraction shows a sinusoidal variation from 7.8 % to 8.3 %, which is in a good agreement with CH_4 mass flow variation.

For reasons of clarity, the temperatures are not displayed in the diagrams. It can be said that the temperature profiles follow the H_2O profiles and reach values of around 1750 K at a HAB of 25.5 mm. This is in good agreement with the results of the simulation which predicts temperatures of 1710 K for the phase angle of 0° and 1740 K for 180° at that HAB. This change in temperature is hardly detectable with the given measurement uncertainty. The flame is not expected to reach the adiabatic equilibrium within the detected HAB. This is evident from the considerable amounts of CO and H_2 still present at that HAB. According to the simulation, the adiabatic temperature will be reached far behind the imaged range of HAB (higher than 400 mm). At adiabatic equilibrium, the change in equivalence ratio would correspond to a temperature change of 40 K.

From the concentration profiles, the section of the CH_4 consumption can be determined to ~6 mm. With the afore estimated velocity of the unburned gas, it takes the gas flow 6.25 ms to cover this distance, not taking into account the acceleration in the preheat zone. During that time, the CH_4 mole fraction varies by about 0.0005 at a pulse frequency of 10 Hz, simplified considering a linear increase (or decrease) in the CH_4 mole fraction of 0.004 during half a period. Therefore, the CH_4 variation in the distance of the CH_4 consumption of 6 mm due to the pulsation is negligible for the state of one phase angle.

4 Summary and Outlook

A novel type of burner has been presented, which enables the stabilization of laminar premixed low pressure flames with periodically changing equivalence ratio Φ. The variation of Φ was achieved by pulsed injection of CH_4 through a multi-tube arrangement into the premixed flow of CH_4/air. For the application of optical and laser measuring techniques, the low pressure vessel was equipped with large windows. In addition, a laser beam could be introduced through the burner along the flame axis. For a flame at 69 mbar and an oscillation frequency of 10 Hz, phase-correlated measurements were performed using laser Raman scattering and OH* chemiluminescence imaging. Due to the good reproducibility of the flame, the results from single-shot 1D laser Raman scattering could be averaged over 300 shots at each phase angle, yielding temperature and major species concentrations along a line of 7 mm length through the flame front. By matching the flow velocity, burner geometry and pressure, the fresh gas exhibited variations of Φ in flow direction up to and including the flame front, whereas concentration gradients in the horizontal plane were completely smoothed out by molecular diffusion. This was experimentally confirmed by 2D Raman imaging measurements of the CH_4 distribution in a vertical plane within the fresh gas flow. Without pulsed injection, the flame had an equivalence ratio of $\Phi = 0.86$ and the pulsation resulted in an increase of the CH_4 flow by 5.4 %. The phase-correlated measurements showed that the flame front moved by about 1.5 mm during an oscillation cycle as a result of the mixture-related change of the laminar flame speed. Numerical simulations with a one-dimensional code for instationary flames including detailed chemistry and transport showed a good agreement with the measured concentration profiles.

The largest uncertainty in the evaluation of the Raman signal arises from the calibration procedure. These uncertainties mainly lead to systematic deviations and periodic changes in the flame structure should still be detectable. The results that are presented in this paper were obtained from flames with a relatively small oscillation in the CH_4 concentration of 5.4%. This made it difficult to detect periodic deviations especially in the concentrations of the product and therefore the temperature in the burned gas. On the other hand, the displacement of the flame due to the imposed oscillation was clearly visible as well as the change in the CH_4 concentration in the fresh gas.

Currently, measurements are performed with higher amplitudes and pulsation rates in order to study the influence of the oscillation frequency on the transport and chemistry within the reaction zone. This will also include strong disturbances that lead to local extinction. With the exemplary results presented here, it could be demonstrated that the experimental setup and the measuring techniques as well as the simulation tool are well-suited for the investigation of the response of a premixed flame front to periodic variations of the equivalence ratio. The results from these measurements and a detailed comparison with results from numerical simulations will be presented in an upcoming paper. The expected findings can be transferred to models describing flames with practical relevance like lean premixed gas turbine flames with respect to thermo-acoustic instabilities.
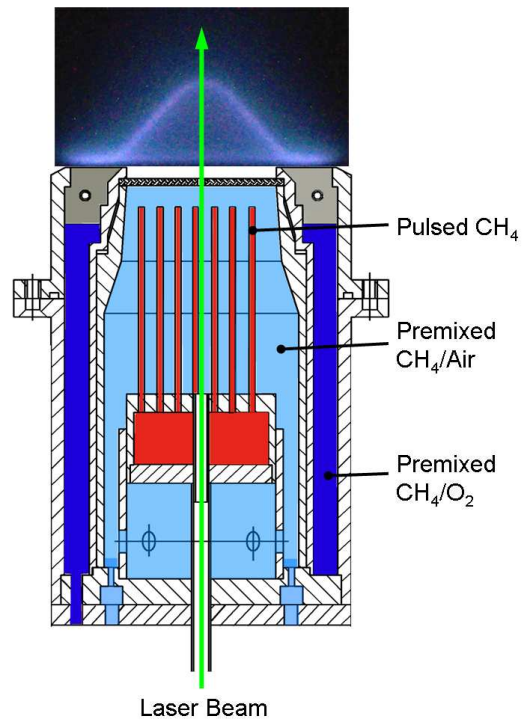
5 Acknowledgements

References

1. S. M. Correa, Combust. Sci. Technol. **87**, 329 (1993).
2. A. H. Lefebvre, *Gas Turbine Combustion* (Taylor & Francis, Philadelphia, 1999).
3. J. J. Keller, AIAA J. **33**, 2280 (1995).
4. E. C. Fernandes, M. V. Heitor, in *Unsteady Combustion*, ed. by F. Culick, M. V. Heitor, J. H. Whitelaw (Kluwer Academic Publishers Group, Dordrecht, 1996), pp. 1-16.
5. C. O. Paschereit, E. Gutmark, W. Weisenstein, Combust. Sci. Technol. **138**, 213 (1998).
6. S. Candel, P. Combust. Inst. **29**, 1 (2002).
7. N. Syred, Prog. Energ. Combust. **32**, 93 (2006).
8. T. S. K. Preetham, T. Lieuwen, AIAA 2006-960 (2006).
9. M. Zhu, A. P. Dowling, K. N. C. Bray, J. Eng. Gas Turb. Power **124**, 20 (2002).
10. T. Lieuwen, J. Propul. Power **19**, 765 (2003).
11. T. Sattelmayer, J. Eng. Gas Turb. Power **125**, 11 (2003).
12. K. Schildmacher, R. Koch, H. Bauer, Flow Turbul. Combust. **76**, 177 (2006).
13. W. Meier, P. Weigand, X. R. Duan, R. Giezendanner-Thoben, Combust. Flame **150**, 2 (2007).
14. R. Sankaran, H. G. Im, P. Combust. Inst. **29**, 77 (2002).
15. Y. M. Marzouk, A. F. Ghoniem, H. N. Najm, P. Combust. Inst. **28**, 1859 (2000).
16. R. Lauvergne, F. N. Egolfopolous, P. Combust. Inst. **28**, 1841 (2000).
17. K. König, U. Maas, Proceedings of the European Combustion Meeting (ECM), paper 80 (2005).
18. K. König, V. Bykov, U. Maas, Flow Turbul. Combust., in print.
19. A. Y. Klimenko, A. G. Class, Combust. Sci. Technol. **160**, 23 (2000).
20. A. Y. Klimenko, A. G. Class, Combust. Sci. Technol. **174**, 1 (2002).
21. A. G. Class, B. J. Matkowsky, A. Y. Klimenko, J. Fluid Mech. **491**, 11 (2003).
22. A. G. Class, B. J. Matkowsky, A. Y. Klimenko, J. Fluid Mech. **491**, 51 (2003).
23. Y. Bronner, Report No. FZKA 7287, Forschungszentrum Karlsruhe (2007).
24. A. C. Eckbreth, *Laser Diagnostics for Combustion Temperature and Species* (Taylor & Francis, New York, 1996).
25. R. S. Barlow, C. D. Carter, R. W. Pitz, in *Applied Combustion Diagnostics*, ed. by K. Kohse-Hinghaus, J. B. Jeffries (Taylor & Francis, New York, 2002), pp. 384-407.
26. L. Wehr, W. Meier, P. Kutne, C. Hassa, P. Combust. Inst. **31**, 3099 (2007).
27. W. Meier, S. Prucker, M. Cao, W. Stricker, Combust. Sci. Technol. **118**, 293 (1996).
28. A Chemical Equilibrium Program for Windows, www.gaseq.co.uk
29. V. N. Nori, J. M. Seitzman, AIAA 2007-466 (2007).
30. N. Docquier, S. Candel, Prog. Energ. Combust. **28**, 107 (2002).
31. J. G. Lee, D. A. Santavicca, J. Propul. Power **19**, 735 (2003).
32. G. P. Smith, C. Park, J. Luque, Combust. Flame **140**, 385 (2005).
33. C. J. Dasch, Appl. Optics **31**, 1146 (1992).
34. U. Maas, Ph.D. Thesis, University of Heidelberg, Germany (1988).
35. J. Warnatz, U. Maas, R. W. Dibble, *Combustion* (Springer, Berlin, Heidelberg, New York, 2001).
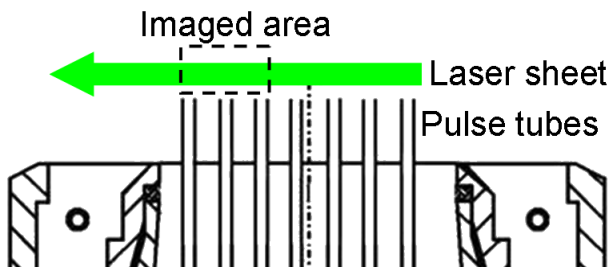
List of Figures

Fig. 1 Schematic drawing of the low pressure burner with a photo of a flame. The colored areas indicate the three separate gas flows for the main flame (light blue), the additional pulsed CH_4 (red) and the flat stabilization flame (dark blue).
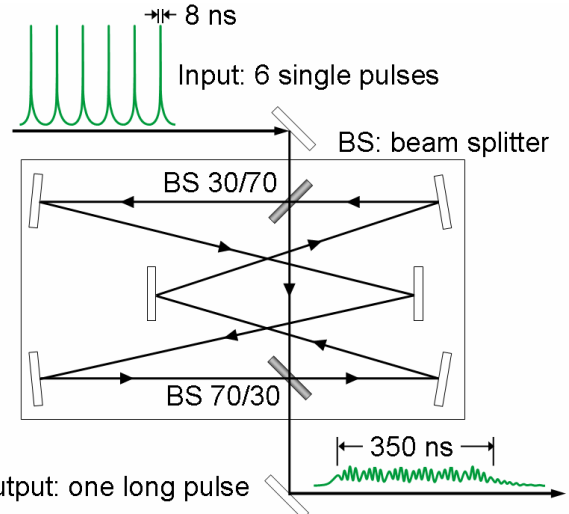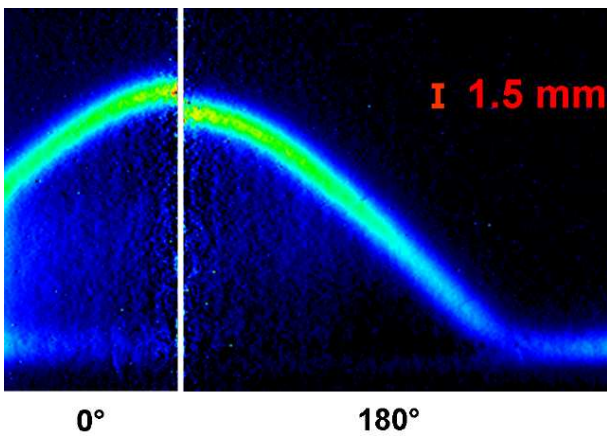

**Fig. 2** Schematic drawing of the pulse stretcher with the courses of the laser beam portions.

**Fig. 3** Schematic drawing of the experimental setup for 2D-Raman measurements of the pulsed CH_4.
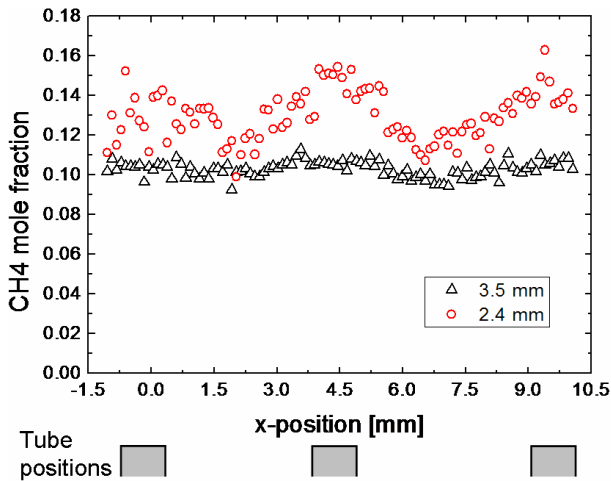
Fig. 4 CH_4 concentrations in horizontal direction at two different heights above the pulse tubes. The horizontal positions of the tubes are indicated underneath.

Fig. 5 OH* distribution at two different phase angles at an oscillation frequency of 10 Hz.
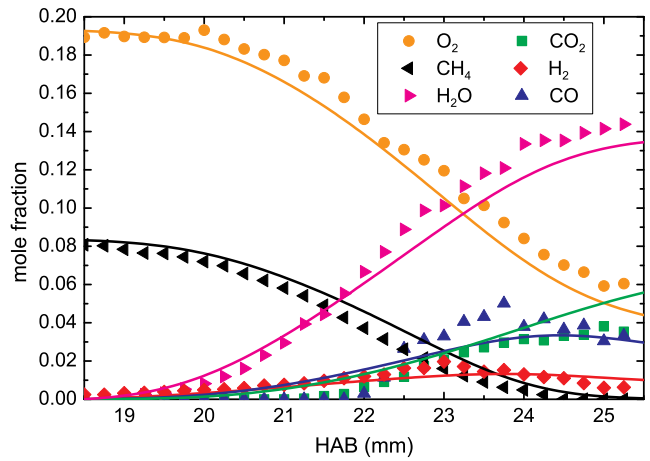
Fig. 6 Concentration profiles of major species across the flame front: 1D Raman experiment (symbols) compared to numerical simulation (lines) at a pulsation phase angle of $0°$.
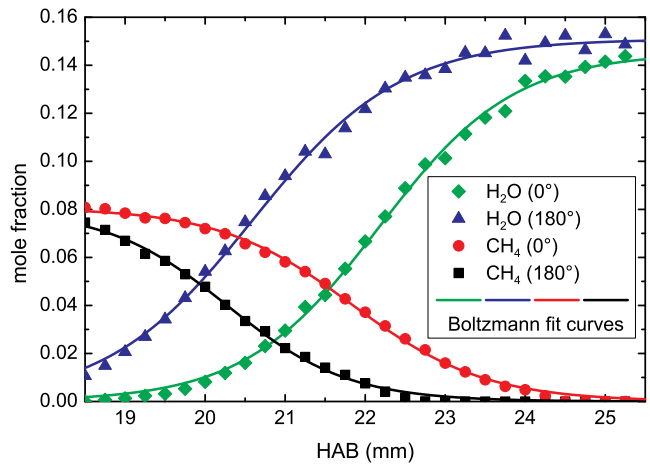
Fig. 7 Methane and water concentration profiles across the flame front at two different phase angles of the mixture fraction oscillation at 10 Hz. The symbols denote the experimental results, the lines are fit curves.